(Received 29 November 2023, Accepted 10 January 2024, Scheduled 25 January 2024)

Enhanced Far-Field Localization Scheme Using Multi-RIS and Efficient Beam Sweeping

Abdulrahaman Kh. Alhafid[1,*], Sedki Younis[2], and Y. E. Mohammed Ali[3]

[1] *Electrical Engineering Department, College of Engineering, University of Mosul, Mosul, Iraq*
[2] *Computer and Information Engineering Department, College of Electronics Engineering, Ninevah University, Mosul, Iraq*
[3] *Computer and Communications Engineering Department, College of Engineering, Nawroz University, Duhok, KRG, Iraq*

ABSTRACT: Future 6G networks are anticipated to use reconfigurable intelligent surfaces (RISs) because of their capability to expand coverage, provide a customizable wireless environment, increase localization accuracy, etc. In this paper, RIS-aided localization is considered with orthogonal frequency division multiplexing (OFDM) and single-input single-output (SISO) downlink system in millimeter-wave (mmWave). An efficient beam sweeping (EBS) scheme is proposed accomplished by an RIS to scan the area of interest and estimate the direction of the user equipment (UE), i.e., the signal's angle of departure (AoD). The AoD with the measured signal time of arrival (ToA), from the RIS to the UE, is used to estimate the UE position. The ToA measurements can be obtained by exploiting the OFDM signal, while the beam sweeping can be obtained by carefully designing the RIS phase profile. The first step of the proposed EBS scheme is to scan the whole area of interest with equally spaced beam angles for coarse estimation of AoD. Then, based on this estimation, the RIS is reconfigured to sweep a slight angle's range by narrow beams to refine the AoD estimation. Besides, a multi-RIS scenario is proposed, and leveraging the EBS and the consensus fusion method is used to obtain accurate position estimation. Simulation results demonstrate that the proposed EBS in single and multi-RIS scenarios enhances positioning accuracy compared to linear beam sweeping (LBS) methods. Also, the impact of increasing the number of RIS elements and number of sweeping beams, as well as the number of RISs, is investigated thoroughly via numerical simulations. Furthermore, the achievable localization accuracy is assessed using the positioning error bound (PEB).

1. INTRODUCTION

In the future generation of communication systems, location awareness will be essential due to the great spread of intelligent applications such as internet-of-things, autonomous vehicles, unmanned aerial vehicles, and self-navigation robots [1, 2]. In communication systems with high carrier frequency, such as 6G, the line-of-sight (LoS) links are easily blocked by obstruction. The LoS is crucial for localization techniques; without LoS, accurate localization becomes difficult. Since the propagation environment plays a significant role in wireless localization, the multipath may not be enough to ensure accuracy in these situations [3]. So, to improve localization capacity in the 6G era, much research has recently been focused on reconfigurable intelligent surfaces (RISs) for localization thanks to their ability to control the propagation environment to some extent [4–6]. In particular, the RIS is envisioned as a flat surface made up of meta-materials with sub-wavelength elements; each element can be individually programmed to perform a desired transformation on an incoming signal to control the wireless propagation channel [6–9]. On the other hand, the RIS can achieve passive beamforming thus offering competitive advantages [10]. In passive beamforming, RIS elements intelligently control the reflecting phase shifts to generate coherent superposition of reflected signals in a desired direction [11, 12]. So, using the passive beamforming with other measurements can be exploited to perform and enhance the UE localization.

RIS assisted localization has been studied in several recent research. Using the enriched radio measurements, the authors in [5] and [13] investigate the use of large RIS in near-field localization using efficient tile selection methods. A far-field RIS-assisted localization and synchronization process was examined in [14] for a single-input single-output (SISO) system. A received signal strength (RSS)-based positioning approach in far-field propagation is proposed by in [15]. The authors in [16] examined the design of the phase profile for a single RIS to dynamically steer the beam sweep over a specific area of interest. The localization is achieved via estimating the angle of departure (AoD) in conjunction with time of arrival (ToA) with the adoption of cooperative communication to improve the precision of localization.

In this paper, an enhanced RIS assist wireless localization system leveraging beamforming is proposed. The RIS is designed to perform an efficient beam sweeping (EBS) to scan the area of interest for the estimation of AoD of the reflected signal towards the UE. Also, the ToA of the signal from the RIS to the UE is estimated to be used with the AoD in the proposed localization algorithm. The proposed EBS is considered for single and multi-RIS scenarios in which the consensus-based fusion is used to combine the position estimations of different measure-

* Corresponding author: Abdulrahaman Kh. Alhafid (abdulrhman.alhafid@uomosul.edu.iq).

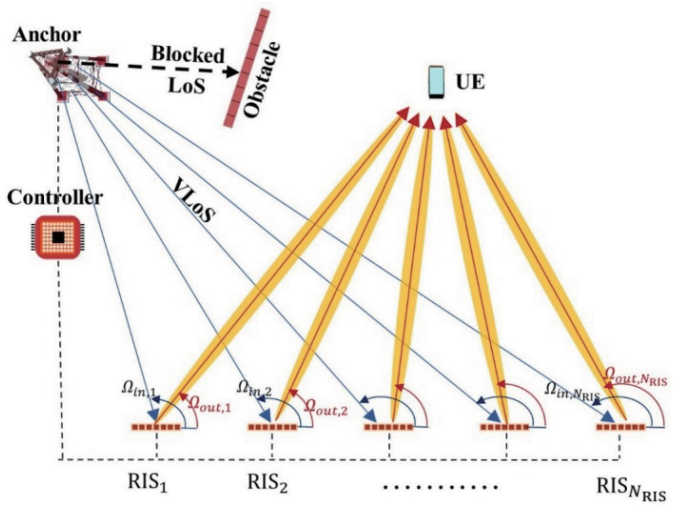

FIGURE 1. An illustration of the system model.

ments. In addition, the positioning error bound (PEB) is derived to evaluate the achievable positioning accuracy considering the effects of various design parameters on localization accuracy.

Notations: The vector is represented by a lowercase bold **a**, whereas the matrix is represented by an uppercase bold **A**. The element in matrix **A** located in the i^{th} row and j^{th} column is denoted by $A_{i,j}$. The operations diag (**a**) and vec (**A**) designate the generation of a diagonal matrix from a vector **a** and the vectorization of a matrix **A**, respectively. The trace of the matrix **A** is denoted by $Tr\,(\mathbf{A})$, and the norm of the vectors and statistical expected value operators are denoted as $\|.\|$ and $\mathbb{E}\,(.)$, respectively.

2. OVERALL SYSTEM MODEL

The RIS-aided localization system model considered in this paper is depicted in Figure 1. We consider a SISO system model with base station (anchor[1]), user equipment (UE), and N_{RIS} of reconfigurable intelligent surfaces (RISs). The anchor and the RISs are located at known positions denoted by $\mathbf{p}_A$ and $\mathbf{p}_{R_i}$, $i = 1, 2 \ldots, N_{RIS}$, respectively whereas $\mathbf{p}_U$ indicates the unknown position of the UE which is to be estimated, where $\mathbf{p}_A$, $\mathbf{p}_{R_i}$ and $\mathbf{p}_U \in \mathbb{R}^{2\times 1}$. The anchor transmits orthogonal frequency division multiplexing (OFDM) based signal to UE in millimeter-wave (mmWave) band using virtual line-of-sight (VLoS) path through the RIS/RISs as depicted in Figure 1. The LoS path is not available due to blockage between the anchor and the UE. It has been assumed that the OFDM signal transmits T pilot symbols, $t = 1, 2, \ldots T$, each with N_{sc} subcarriers, $n = 1, 2, \ldots N_{sc}$ separated by Δ_f. Each RIS consists of $N_e = N_r \times N_c$ elements with uniform linear array (ULA) arrangement, where N_r and N_c are the numbers of RIS elements in each row and column, respectively.

The angle-of-arrival (AoA) at the i^{th} RIS from the anchor is denoted by $\Omega_{in,i}, \forall i$. Similarly, the AoD from the i^{th} RIS toward the UE is denoted by $\Omega_{out,i}, \forall i$. Since the locations of the anchor and the RISs are known and fixed, the values of $\Omega_{in,i}$ can be easily obtained by using some geometrical relationships. Our goal in this study is to estimate the values of $\Omega_{out,i}, \forall i$ and the distance from the RIS to the UE then use them to estimate the locations of the UE.

With the assumption that the RISs are located at (x, z) plane, and the inter-element distance is d, which is half-wavelength [17], the positions of elements for the i^{th} RIS could be expressed as,

$$\mathbf{p_{e,i}} = \mathbf{p}_{R_i} + d\left[\left(n_c - \frac{(N_c-1)}{2}\right), 0, \left(n_r - \frac{(N_r-1)}{2}\right)\right] \quad (1)$$

where $n_c = 1,\ 2,\ \ldots\ N_c$, and $n_r = 1,\ 2,\ \ldots\ N_r$.

Regarding the channel model, due to the assumption of blockage for LoS path between the anchor and the UE, it is mainly focused on the VLoS channel between the anchor and the UE through the RISs. On the other hand, the NLoS paths in mmWave systems often have very little power compared with VLoS; therefore, they are quite unreliable for localization purposes [18–20]. The propagation channel from the anchor to the i^{th} RIS for one OFDM symbol transmission can be expressed as [14],

$$\mathbf{h}_{ar,i} = g_{ar,i}\mathbf{d}\,(\tau_{ar,i})\,\mathbf{a}\,(\Omega_{in,i}) \in \mathbb{C}^{N_{sc}\times N_e} \quad (2)$$

where $g_{ar,i}$ is the channel gain between the anchor and the i^{th} RIS expressed by the distance between the anchor and the RIS, $d_{ar,i} = \|\mathbf{p}_{R,i} - \mathbf{p}_A\|$ and by the path loss exponent μ as,

$$g_{ar,i}\,(\text{dBm}) = -10\mu \log_{10}(d_{ar,i}) \quad (3)$$

while the delay effect of the propagation distance from the anchor to the i^{th} RIS is captured by the vector $\mathbf{d}\,(\tau_{ar,i})$ as,

$$\mathbf{d}\,(\tau_{ar,i}) = \left[1, e^{-j2\pi\Delta_f\tau_{ar,i}}, \ldots, e^{-j2\pi(N_{sc}-1)\Delta_f\tau_{ar,i}}\right]^\top \in \mathbb{C}^{N_{sc}\times 1} \quad (4)$$

[1]The term "base station" refers to the transceiver that offers connectivity in wireless communication systems. The term "anchor" is used to indicate a geometry reference for localization purpose in addition to its work of wireless connectivity, so it will be used in this paper as in many references like [8, 26].

where $\tau_{ar,i} = d_{ar,i}/c$, c is the speed of the light, and $\mathbf{a}(\Omega_{in,i})$ in (2) is the incident steering vector response at the i^{th} RIS,

$$\mathbf{a}(\Omega_{in,i}) = \exp\left(-j\mathbf{k}(\Omega_{in,i})^{\top}\mathbf{p}_{e,i}\right) \in \mathbb{C}^{1\times N_e} \quad (5)$$

where $\mathbf{p}_{e,i}$ is the relative RIS element position as expressed in (1), and $\mathbf{k}(\Omega_{in,i})$ is wavenumber vector which expressed, in general, by elevation $(\theta_{in,i})$ and azimuth $(\varphi_{in,i})$ angles and can be defined as [21, 22],

$$\mathbf{k}(\Omega_{in,i}) = -\frac{2\pi}{\lambda}[\sin\theta_{in,i}\cos\varphi_{in,i}\sin\theta_{in,i}\sin\varphi_{in,i}\cos\theta_{in,i}] \in \mathbb{R}^{1\times 3} \quad (6)$$

Similarly, the propagation channel response from the i^{th} RIS to the UE can be expressed as,

$$\mathbf{h}_{ru,i} = g_{ru,i}\mathbf{d}(\tau_{ru,i})\,\mathbf{a}(\Omega_{out,i}) \in \mathbb{C}^{N_{sc}\times N_e} \quad (7)$$

where $g_{ru,i}$, $\mathbf{d}(\tau_{ru,i})$, and $\mathbf{a}(\Omega_{out,i})$ are the channel gain, delay effect of the propagation distance, and the exit steering vector response from the i^{th} RIS, respectively, which can be defined in the similar ways to that in (3) to (6) as,

$$g_{ru,i}(\text{dBm}) = -10\mu\log_{10}(d_{ru,i}) \quad (8)$$

where $d_{ru,i} = \|\mathbf{p}_U - \mathbf{p}_{R,i}\|$, while the delay effect of the propagation distance from the i^{th} RIS to the UE is expressed as,

$$\mathbf{d}(\tau_{ru,i}) = \left[1, e^{-j2\pi\Delta_f\tau_{ru,i}}, \ldots, e^{-j2\pi(N_{sc}-1)\Delta_f\tau_{ru,i}}\right]^{\top} \in \mathbb{C}^{N_{sc}\times 1} \quad (9)$$

$$\mathbf{a}(\Omega_{out,i}) = \exp\left(-j\mathbf{k}(\Omega_{out,i})^{\top}\mathbf{p}_{\mathbf{e,i}}\right) \in \mathbb{C}^{1\times N_e} \quad (10)$$

where $\tau_{ru,i} = d_{ru,i}/c$ and $\mathbf{k}(\Omega_{out,i})$ is the wavenumber vector which is expressed like (6) as,

$$\mathbf{k}(\Omega_{out,i}) = -\frac{2\pi}{\lambda}[\sin\theta_{out,i}\cos\varphi_{out,i}\sin\theta_{out,i}\sin\varphi_{out,i}\cos\theta_{out,i}] \in \mathbb{R}^{1\times 3} \quad (11)$$

The effect of each RIS on the incident signal at each symbol time t can be described by the diagonal matrix $\mathbf{W}_{t,i}^{\text{diag}} \in \mathbb{C}^{N_e\times N_e}$ of the vectorized RIS phase profile $\mathbf{w}_{t,i}^{vec}\mathbb{C}^{1\times N_e}$ from the RIS phase profile matrix $\mathbf{W}_{t,i}\mathbb{C}^{N_r\times N_l}$, i.e.,

$$\mathbf{W}_{t,i}^{\text{diag}} = \text{diag}\left(\mathbf{w}_{t,i}^{vec}\right) = \text{diag}\left(\text{vec}\left(\mathbf{W}_{t,i}\right)\right) \quad (12)$$

$$\text{vec}\left(\mathbf{W}_{t,i}\right) = \left(e^{j2\pi\theta_{1,i}}, e^{j2\pi\theta_{2,i}}, \ldots, e^{j2\pi\theta_{N_e,i}}\right) \quad (13)$$

The cascaded propagation channel from anchor to the RIS then to the UE for all the T OFDM symbols, denoted by $\mathbf{H}_{VLoS,i}$ which include the RIS effect $\mathbf{W}_{t,i}^{\text{diag}}$ can be written as,

$$\mathbf{H}_{VLoS,i} = \mathbf{h}_{ru,i}^{\top}\mathbf{W}_{t,i}^{\text{diag}}\mathbf{h}_{ar,i} \in \mathbb{C}^{N_{sc}\times T} \quad (14)$$

The proposed system assumes that the RIS controller manipulates and adjusts only the phases of the reflected signal, while the magnitude of the reflection coefficient remains unity, which is following the widely used assumptions, such as in [19, 23, 24]. So, the reflection coefficient for an RIS element can be expressed as,

$$w_{t,e} = \Upsilon e^{j\psi_{t,e}} \quad (15)$$

where Υ and $\psi_{t,e}$ are, respectively, the amplitude and phase of the reflection coefficient for the n_e^{th} element. Based on the above, the received signal at UE from the i^{th} RIS can be expressed as,

$$\mathbf{Y}_i = \mathbf{H}_{VLoS,i}x + \mathbf{N} \quad (16)$$

where the observation signal $\mathbf{Y}_i$ is a matrix of $\in\mathbb{C}^{N_{sc}\times T}$; x denotes the signal transmitted by the anchor[2]; $\mathbf{N}$ denotes the additive white Gaussian noise (AWGN) which is circular symmetric complex Gaussian $\mathbf{N}\sim CN\left(0,\sigma^2\right)$ with zero mean and variance σ^2.

3. PROPOSED LOCALIZATION SYSTEM IN FAR-FIELD USING RIS BEAM SWEEPING

In this section, three models for UE localization are investigated. The first one is a multi-RIS model, which exploits linear beam sweeping (LBS) accomplished by the RISs together with the ToAs. In contrast, the second one is a single RIS model which uses the proposed EBS together with the ToA. Then, the second model is extended to the third model, in which multi-RISs with EBS and ToA are used. In the following subsections, each model will be explained in detail.

3.1. Localization Model Using Multi-RIS with ToA and LBS

In this scenario, two stages are used to localize the UE. In the first stage, the ToA for the path between each RIS and the UE is estimated by exploiting the OFDM observation signal in (16). This can be accomplished, as in [8, 14], by finding the IFFT of the received frequency domain symbols with oversampling factor of N_{os}, then evaluating the peak value of the obtained time domain signal as,

$$\hat{\tau}_{VLoS,i} = \arg\max_{j}\left(\text{IFFT}(\mathbf{Y}_i)\right),\ j\in[0,(N_{os}\times N_{sc}-1)] \quad (17)$$

Then, Quasi-Newton algorithm could be used to refine the estimation and attain sufficient accuracy as given in [14].

The RIS phase profile in this stage is designed to use random uniform distribution to determine the phase values for the RIS elements. The reflection phases in (15) is drawn as:

$$\psi_{t,e} = 2\pi\text{rand}(N_e, T) \quad (18)$$

Then, by multiplying the estimated delay $\hat{\tau}_{VLoS,i}$ by the speed of light, distance from the anchor to the UE through the i^{th} RIS will be obtained. Since the RISs and anchor coordinates are known, the estimated distance between the i^{th} RIS and UE, i.e., $\hat{d}_{ru,i}$, is obtained by deducting RIS to anchor distance $d_{ar,i}$ from the total distance,

$$\hat{d}_{ru,i} = \hat{\tau}_{VLoS,i}\cdot c - d_{ar,i} \quad (19)$$

[2]Without loss of generality, it is assumed a constant pilot $x = 1$.

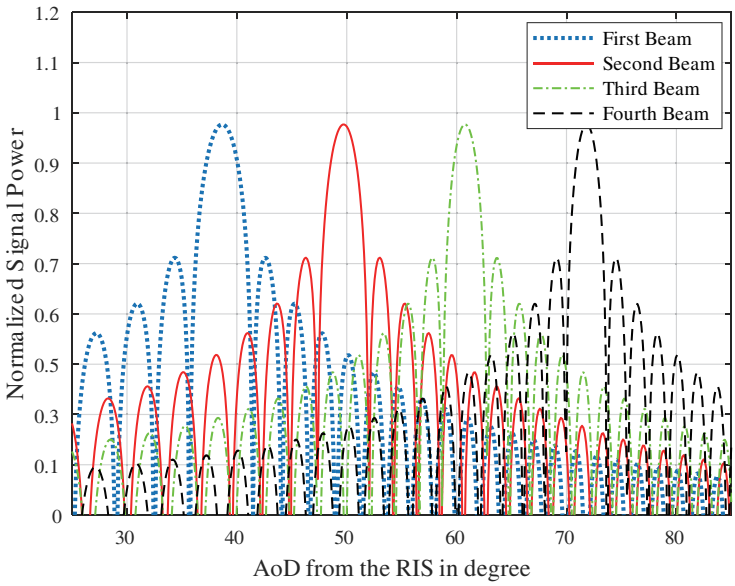

FIGURE 2. An example of four beams distributed for LBS from $\varphi_f = 38.6^\circ$ to $\varphi_l = 82.8^\circ$.

In the second stage, the AoD from each RIS can be estimated following the considerations in [16]. Each RIS is employed to perform a beam sweeping to scan the area of interest with successive beams of equally spaced angles which is the LBS. The AoD is determined by detecting the highest received beam signal at UE. Thus, if the area of interest has first point at angle φ_f and last point at angle φ_l, then the LBS angles φ_s will be at,

$$\varphi_s = \varphi_f + \frac{(2s-1)\,(\varphi_l - \varphi_f)}{2S}, \quad s \in (1, 2, \ldots, S) \tag{20}$$

where S is the total number of the desired beams and s the sequence number of the beams.

The RIS phase profile is configured to direct a narrow beam towards φ_s at each symbol transmission. To fulfill this beamforming, each column of the phase profile matrix takes the same value at each transmission, so each row in the profile matrix is configured as,

$$\begin{aligned} \mathbf{w}_{t,i}^{row} &= \left[1, e^{j2\pi \frac{d}{\lambda}\varphi_{ris}}, \ldots, e^{j2\pi \frac{d}{\lambda}(N_c-1)\varphi_{ris}}\right], \\ \mathbf{w}_{t,i}^{row} &\in \mathbb{C}^{1\times N_c} \end{aligned} \tag{21}$$

where φ_{ris} is the angle used to achieve the desired beamforming. The steering vectors in (5) and (10) along with the wavenumber vectors (6) and (11) in the received signal should be considered to specify the angle φ_{ris}. The elevation angle in the wavenumber vector is 90° resulting in an elimination of the third term in the wavenumber vectors. Also, we assume that the RISs are located at the (x, z) plane, and the second term in the wavenumber vector will be eliminated too. Consequently, φ_{ris} will be as,

$$\varphi_{ris} = \cos(\varphi_i) - \cos(\varphi_r) \tag{22}$$

where φ_i is the known azimuth AoA from the anchor to the RIS, and φ_r is the desired AoD or sweeping angle, i.e., φ_s.

Figure 2 illustrates an example of LBS in an interesting area performed by RIS that contains 64 elements using (20), (21), and (22), and the area of interest is designed to be a square area enclosed by the coordinates as will be illustrated in Subsection 6.1. After completion of the beam sweeping operation by each RIS, the UE will determine the index of the highest received beam signal as in [16],

$$s_{\max,i} = \underset{S\in(1,2,\ldots,S)}{\arg\max} \left\|\mathbf{Y}_{s,i}\right\|^2 \tag{23}$$

where $\left\|\mathbf{Y}_{s,i}\right\|^2$ is the received beam signal power from the i^{th} RIS, an d$s_{\max,i}$ is the index of the highest received beam signal. This index refers to one of the designed angles in (20), i.e., the estimated AoD from the RIS towards the UE. It is assumed that the UE lies at the center of the assigned beam indexed as $s_{\max}$. Then, for each RIS located at $\mathbf{p}_{R_i} = [x_{R_i}, y_{R_i}]$, we can use the estimated ToA, after converting it to $\hat{d}_{ru,i}$, with the estimated $\varphi_{s_{\max},i}$ to localize the UE as,

$$\begin{aligned} \hat{\mathbf{p}}_{U,i} &= \left[x_{R_i} + \hat{d}_{RU}\cos\varphi_{s_{\max,i}}, y_{R_i} + \hat{d}_{RU}\sin\varphi_{s_{\max},i}\right]\ldots \\ & i \in (1,\, 2,\, \ldots, N_{RIS}) \end{aligned} \tag{24}$$

Now, the number of estimations for each UE position is the same as the number of used RISs N_{RIS}, so consensus fusion algorithm is used to find the centroid of the estimated positions.

3.2. Proposed Localization Model Using Single-RIS with ToA and EBS

The localization scenario in this proposed model uses single RIS to estimate the UE location. The two stages used in Subsection 3.1 are also used in this scenario. In the first stage, the

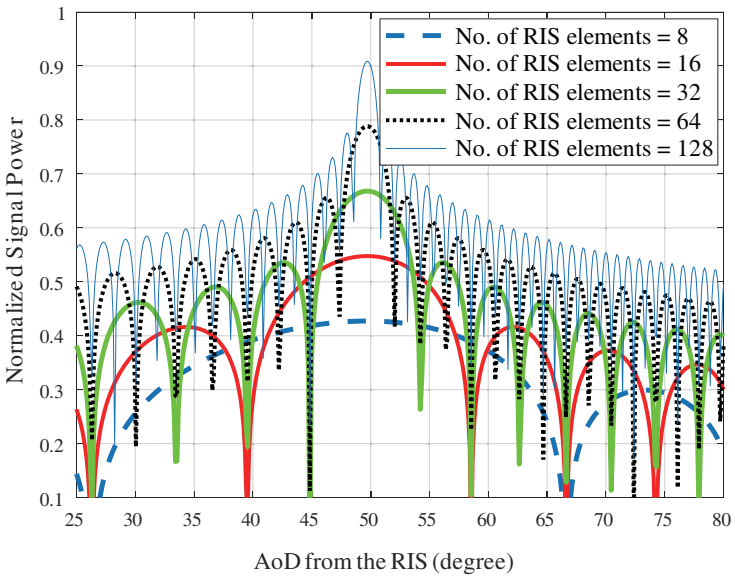

FIGURE 3. Illustration of RIS beam pattern for different numbers of elements.

ToA from the RIS to the UE is estimated like before. In the second stage, the proposed EBS method is performed in two steps. In the first step, an LBS is performed using a small number of beams to scan the whole area of interest and estimate a low resolution AoD using (23) which will be used in the second step of the EBS. The low resolution AoD together with the estimated ToA can be used to obtain a coarse estimation of the UE position using (24). In the second step of the proposed EBS, depending on the low resolution estimated angle, RIS phase profile is designed to direct narrow beams to make beam sweeping around the estimated angle in the first step. Then, using (23) again, a refined AoD estimation can be obtained. At last, equation (24) is used to get the refined localization. Algorithm 1 describes the proposed localization approach.

It is worth mentioning that in the first step of the proposed EBS, the RIS profile is designed to generate successive and relatively wide beams during the LBS, that's to cover the whole area of interest by a small number of beams. This can be achieved by reducing the number of the configured elements by deactivating some elements or configuring each two (or more) neighbor elements by same configuration. In the second step, narrow beams are used to get more refined estimation. Figure 3 is a beam pattern example showing the effect of the number of RIS elements on the beamforming, in which different numbers of RIS elements are configured using (21) to direct a beam towards angle of (49.7°) using (22), and the normalized received power is plotted versus the angles in degrees. The increase in number of RIS elements makes the beam narrower.

3.3. Proposed Localization Model Using Multi-RIS with ToA and EBS

The proposed localization model for single RIS in Subsection 3.2 has been extended to multi-RIS model by using N_{RIS} of RISs as shown in Figure 1. So, the distances between each RIS and the UE will be estimated using (16), (17), and (19). Then each RIS performs EBS, and the low resolution AoDs in addition to the refined AoDs will be estimated using the second stage in Subsection 3.2. Consequently, by using (24), an estimation of UE location for each RIS will be obtained, i.e., the number of estimated positions for the UE is equal to N_{RIS}. So, consensus fusion method is used to get the refined UE position. Algorithm 2 describes this proposed localization approach.

4. PERFORMANCE BOUNDS

The Cramer-Rao Lower Bound (CRLB) for positioning error, which is positioning error bound (PEB), is derived in this section to assess the attainable positioning accuracy which sheds light on the impact of the system parameters on localization accuracy. This PEB is used as a benchmark for the proposed positioning methods and provides a lower bound on the variance of the unbiased estimator [25]. It can be obtained by calculating the Fisher information matrix (FIM) related to the position parameters which are to be estimated. The PEB can be written as [26],

$$\text{PEB} = \sqrt{Tr\left(\mathbf{FIM}_{\mathbf{p}_u}^{-1}\right)} \tag{25}$$

where $\mathbf{FIM}_{\mathbf{p}_u}$ is the FIM for the location parameters $\mathbf{p}_u$. The FIM can be obtained using log-likelihood function of the estimated parameters. In this paper, the estimator parameters vector can be written as,

$$\hat{\mathbf{a}}_{Est} = \left[\hat{\mathbf{d}}_{RU,i}^{\top}, \hat{\boldsymbol{\varphi}}_{RU,i}^{\top}\right]^{\top} \in \mathbb{R}^{2N_{RIS}\times 1},$$
$$i \in (1, 2, \ldots, N_{RIS}) \tag{26}$$

Algorithm 1: Proposed Localization Model Using Single-RIS with ToA and EBS

Input: Anchor position $\mathbf{p}_A$, RISs positions $\mathbf{p}_R$
Objective: Estimate UE position $\hat{p}_U$ and direction $\varphi_{s_{\max}}$
Stage I Estimate distance from RIS to UE, i.e., $\hat{d}_{ru}$
1: **Initialize:** OFDM subcarriers N_{sc}, OFDM symbols T Oversampling factor N_{os}
2: Calculate the IFFT of the received signal
3: Estimate $\hat{\tau}_{VLoS}$ using (17)
4: Calculate RIS to UE distance $\hat{d}_{ru}$ using (19)
Stage II Estimate AoD from RIS towards UE, i.e., φ_{out}
5: **Step 1:** Estimate low resolution angle AoD
6: **Initialize:** Number of wide beams S_{wid} for LBS, first and last angles for area of interest φ_f & φ_l, RIS phase profile
7: Calculate LBS angles φ_s using (20)
8: **for** $s = 1$**to**S_{wid}**do**
9: Assign RIS phase profile according to (21)
10: Perform the LBS
11: **end**
12: Find $s_{\max}$ according to (23)
13: Estimate the low resolution AoD
14: **Step 2:** Estimate fine angle AoD
15: **Initialize:** Number of narrow beams S_{nar} for EBS, RIS phase profile
16: Obtain low resolution AoD from ***Step 1***
17: **for** $s = 1$**to**S_{nar}**do**
18: Assign the RIS phase profile according to (21) and (22)
19: Perform the EBS
20: **end**
21: Find $s_{\max}$ according to (23)
22: Estimate the refined AoD $\varphi_{s_{\max}}$
23: Compute UE position using ToA from Stage I and AoD from Stage II/Step 2 using (24)
Output: The estimated $\hat{p}_U$ & the direction of the UE $\varphi_{s_{\max}}$ w.r.t the RIS

Algorithm 2: Proposed Localization Model Using Multi-RIS with ToA and EBS

Input: Anchor position $\mathbf{p}_A$, RISs positions $\mathbf{p}_{R_i}$
Objective: Estimate UE position $\hat{p}_U$ and direction $\varphi_{s_{\max}}$
1: **for** $i = 1$ **to** N_{RIS} **do**
2: Use ***Algorithm 1/Stage I to estimate the distance*** $\hat{d}_{ru,i}$ ***from the*** i^{th} ***RIS to the UE***
3: Use ***Algorithm 1/ Stage II/ Step 1 to estimate low resolution angle AoD for the*** i^{th} ***RIS.***
4: Use ***Algorithm 1/ Stage II/ Step 2 to estimate the refined angles AoDs*** $\varphi_{s_{\max,i}}$ ***from each RIS towards the UE.***
5: Compute the UE position $\hat{\mathbf{p}}_{U,i}$ using (24)
end
6: Obtain the estimated positions of the UE $\hat{\mathbf{p}}_{U,i}$
7: Use consensus fusion method to find the refined UE position
Output: The final estimation of $\hat{\mathbf{p}}_U$

where $\hat{\mathbf{d}}_{RU,i}$ and $\hat{\boldsymbol{\varphi}}_{RU,i}$ are the estimated distance, obtained from the estimated ToA, from the i^{th} RIS to the UE, and the estimated azimuth angle between the i^{th} RIS and the US, respectively, i.e.,

$$\begin{aligned}\hat{\mathbf{d}}_{RU,i}^{\top} &= \left[\hat{d}_{RU,1}, \hat{d}_{RU,2} \ldots \hat{d}_{RU,N_{RIS}}\right] \\ \hat{\boldsymbol{\varphi}}_{RU,i}^{\top} &= [\hat{\varphi}_{RU,1}, \hat{\varphi}_{RU,2} \ldots \hat{\varphi}_{RU,N_{RIS}}]\end{aligned} \tag{27}$$

The likelihood function of the estimator parameters vector $\hat{a}_{Est}$, can be described as in [27],

$$f\left(\hat{\mathbf{a}}_{Est}\right) = \prod_{i=1}^{N_{RIS}} \frac{1}{2\sqrt{2}\pi^3 \sigma_{d_{RU,i}} \sigma_{\varphi_{RU,i}}} e^{-\left[\frac{\left(\hat{d}_{RU,i} - d_{RU,i}\right)^2}{2\sigma^2_{d_{RU,i}}} + \frac{\left(\hat{\varphi}_{RU,i} - \varphi_{RU,i}\right)^2}{2\sigma^2_{\varphi_{RU,i}}}\right]} \tag{28}$$

TABLE 1. Simulation parameters.

Parameter	Value
Carrier frequency f_l	28 GHz
No. of OFDM subcarriers N_{sc}	128
No. of OFDM pilot transmissions T	8–256
Subcarrier spacing Δf	120 kHz
Transmitted power P_T	23 dBm
No. of RIS elements	32–512
Noise power spectral density N_o	-170 dBm/Hz
path loss exponent μ	2.08
IFFT oversampling N_{os}	8
No. of RISs N_{RIS}	1–5

Taking into consideration the fact that the estimates of the $d_{RU,i}$ and $\varphi_{RU,i}$ are unbiased, i.e., $\mathbb{E}\left(\hat{d}_{RU,i}\right) = d_{RU,i}$ and $\mathbb{E}\left(\hat{\varphi}_{RU,i}\right) = \varphi_{RU,i}$, and using same procedures in [27], the FIM can be expressed as,

$$\mathbf{FIM}_{\mathbf{p}_u} = \mathbb{E}\left(\mathbf{D}_{Est}^{\top}\mathbf{R}_{Est}\mathbf{D}_{Est}\right) \tag{29}$$

where,

$$\mathbf{D}_{Est}=\text{diag}\left(\sigma_{d_{RU,1}}^{-2},\ldots,\sigma_{d_{RU,N_{RIS}}}^{-2},\sigma_{\varphi_{RU,1}}^{-2},\ldots,\sigma_{\varphi_{RU,N_{RIS}}}^{-2}\right) \tag{30}$$

$$\mathbf{R}_{Est}=\begin{bmatrix} \frac{x_U-x_{R_1}}{d_{RU,1}} & \frac{y_U-y_{R_1}}{d_{RU,1}} \\ \vdots & \vdots \\ \frac{x_U-x_{R_{N_{RIS}}}}{d_{RU,N_{RIS}}} & \frac{y_U-y_{R_{N_{RIS}}}}{d_{RU,N_{RIS}}} \\ \frac{y_U-y_{R_1}}{s_1^2} & \frac{x_U-x_{R_1}}{s_1^2} \\ \vdots & \vdots \\ \frac{y_U-y_{R_{N_{RIS}}}}{s_{N_{RIS}}^2} & \frac{x_U-x_{R_{N_{RIS}}}}{s_{N_{RIS}}^2} \end{bmatrix} \tag{31}$$

$$s_i=\sqrt{\left(x_U-x_{R_i}\right)^2+\left(y_U-y_{R_i}\right)^2}\ldots i\in(1,2,\ldots,N_{RIS}) \tag{32}$$

5. COMMENT ON OTHER ALGORITHMS THAT INVOLVE TOA AND AOD MEASUREMENTS.

The localization scheme proposed in this paper utilizes the ToA and AoD estimation, where two-stage estimation is investigated via efficient beam sweeping. In order to compare the proposed algorithm with other localization schemes that have used ToA and AoD estimations to determine the position of the UE, we consider the estimation procedure discussed in [28]. Regarding the hardware setup, the estimation procedure in [28] requires adopting a hybrid RIS that is equipped with a radio frequency (RF) chain to facilitate the estimation of forward, backward, and LoS channels. For a fair comparison with [28] and considering the scenario in Figure 1, $\hat{\tau}_{VLoS}$ can be estimated using the same procedure described in Subsection 3.1, while the main difference with [28] is the AoD estimation. In [28], the AoD is estimated by solving the maximum likelihood (ML) optimization problem which is computationally expensive compared with the beam sweeping scheme used in this paper. Although the proposed scheme is computationally efficient, it is clear that it will be at the expense of requiring more transmissions during the beam-sweeping phase.

6. SIMULATION RESULTS AND ANALYSIS

In this section, we conduct numerical analysis to assess the performance of the proposed EBS models in Section 3. The performance of the proposed models is compared with the LBS under different values of the parameters. We consider the cumulative distribution function (CDF) and root mean squared error (RMSE) as performance metric estimated on 1000 independent Monte Carlo trials. We first investigate the performance of the LBS for multi-RIS model. Then the performance of the proposed EBS of single-RIS model is evaluated and compared with the conventional LBS for single-RIS. Finally, the proposed EBS for multi-RIS model is investigated and compared with its LBS counterpart. Also, the impact of the number of RISs and number of beams for LBS and EBS are thoroughly studied.

6.1. Simulated Scenarios

The parameters used in the simulation are detailed in Table 1. The considered values are consistent with the suggested literature such as in [14, 16, 23, 24, 29, 30] A system with anchor, UE and $N_{RIS}\in(1,2,\ldots,5)$ of RISs is considered for investigating the performance of the proposed models. The location of anchor $\mathbf{p}_A = (-50, 80)$, with the UEs assumed to uniformly distributed inside the area of interest. The area of interest is chosen to be a square area surrounded by the four coordinates: $(10, 40)$, $(50, 40)$ $(50, 80)$ and $(10, 80)$. The RISs positions $\mathbf{p}_{R_i}$ are (x_i), where $x_i = 5\,(i-3)$ and $i \in (1, 2, \ldots, 5)$. Note that all the dimensions are in meters.

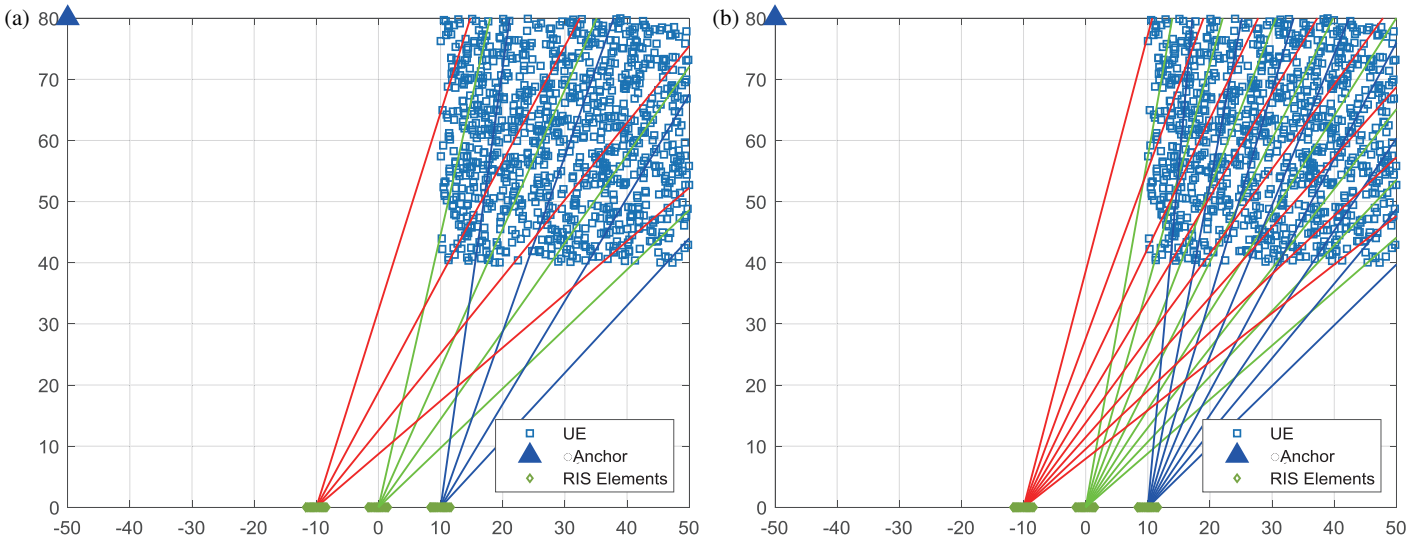

FIGURE 4. Examples of LBS for three RISs (a) four beams (b) eight beams.

6.2. Results and Discussion

6.2.1. Performance of the Proposed LBS with Multi-RIS Model

The simulation results in this part investigate the performance of multi-RIS model that uses LBS which is described in Subsection 3.1. Before introducing the investigation of this model, an example of LBS is illustrated in Figure 4 using the angles φ_s in (20) and phase profile in (21). This figure shows the positions of the RISs at the x-axis and the anchor at the y-axis. The LBS for three RISs, each configured to sweep the area of interest, with four and eight beams are shown in subplots (a) and (b), respectively.

In Figure 5, the performance of the localization is plotted as CDF for different numbers of RISs, ($N_{RIS} = 2$ to 5) and compared with a single RIS scenario. In addition, the impact of the beam numbers of LBS is considered, where the number of beams was 4, 8, 16, 32, 64 in subplots (a) to (e), respectively. The CDF curves demonstrate that the increase of the number of beams and/or the number of RISs enhance the localization performance. So, when five RISs are used, the performance enhancement is about (45 to 50)% compared with the use of one RIS at 90% of the CDF and about (50 to 55)% at the 67% of CDF. In specific, by using five RISs with 64 beams, the error is smaller than 20 cm and 14 cm at 90% and 67% of the CDF, respectively.

Figure 6 shows the RMSEs of the estimation of the UE position as a function of the number of beams used for LBS for different numbers of RISs. By comparing the RMSEs in Figure 6, it clearly emerges that the use of more beams and more RISs yields more accurate estimates of the UE positions than the single RIS case. As expected, in this scenario, the use of five RISs, each with 64 beams of LBS, outperforms all the other cases, but it involves an exhaustive LBS with a large number of transmissions. So, the use of 32 beams with five RISs may provide a good tradeoff that can achieve about 20 cm of localization accuracy. Note that the results in both Figures 5 and 6 are based on RISs with 128 elements.

6.2.2. Performance of the Proposed EBS with Single-RIS Model

In this section, the performance of the proposed EBS method for RIS aided localization is studied. We consider four wide beams that scan the area of interest in a linear fashion and consider the number of beams for EBS to be from 4 to 16. In other words, we set ($S_{wid} = 4$) and ($S_{nar} = 4$ to 16), respectively, in the first and second steps of stage II in Algorithm 1. To illustrate the EBS scenario, a snapshot is taken for one UE in the case of $S_{wid}= 4$ and $S_{nar}= 4$ and shown in Figure 7. In this figure, the dashed red lines represent the centers of the beams that scan the whole area of interest to estimate the low-resolution angle, and the coarse localization of the UE is denoted by the red point. Then based on the previous step, the EBS is performed using four beams in which their centers are plotted in blue lines to make the estimated position closest to the real position as indicated by green color square and blue color square, respectively. In this snapshot example, the estimation error between the real position and the coarse estimation is equal to 3.51 m which is not quite accurate. After the second step of the EBS is performed, the estimation error between the real position and the fine estimation is equal to 46 cm. Consequently, the RMSE of the localization versus the number of beams is depicted in Figure 8 for different numbers of RIS elements. Figure 8 shows that as the total number of beams increases, the localization error decreases. In contrary, Figure 9 shows the RMSE of positioning versus the number of RIS elements. It is noted that when the RIS elements are greater than 256, the slope of the estimation tends to floor especially when the total number of beams is equal to 20, in which the error decreases from 38 cm to 30 cm.

To benchmark the proposed method in Algorithm 1, we compare the proposed EBS with the LBS in Figure 10 and Figure 11. Figure 10 shows the RMSE versus the number of beams for different numbers of RIS elements. Figure 11 depicts a comparison of RMSE of the proposed EBS with the LBS versus RIS elements. The proposed EBS method outperforms the conven-

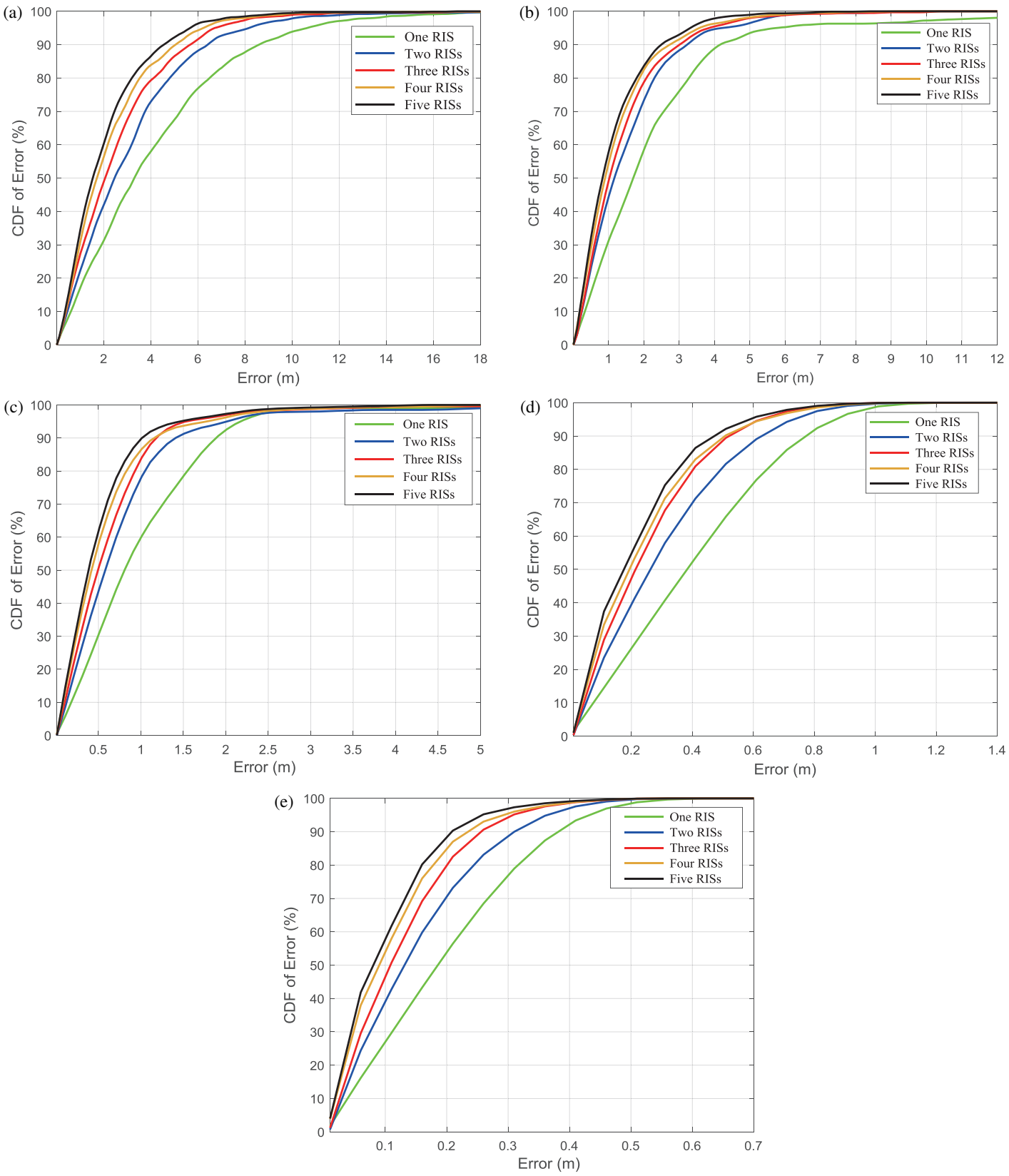

FIGURE 5. CDF of localization error using multi-RIS with ToA and LBS for different numbers of beams (a) 4-beams, (b) 8-beams, (c) 16-beams, (d) 32-beams and (e) 64-beams.

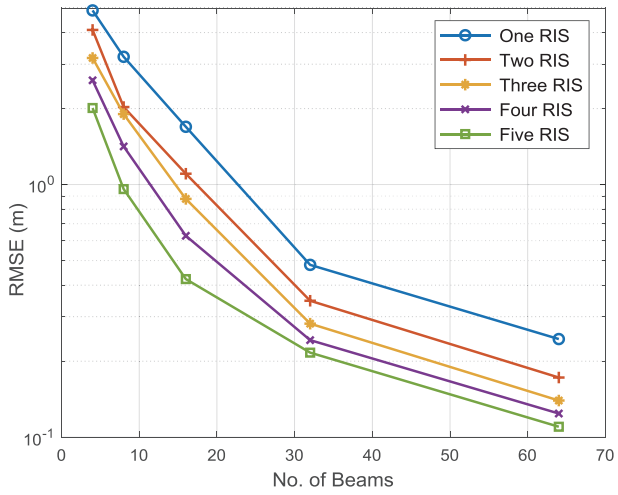

FIGURE 6. RMSEs of localization as a function of beam's numbers for single and multi RISs.

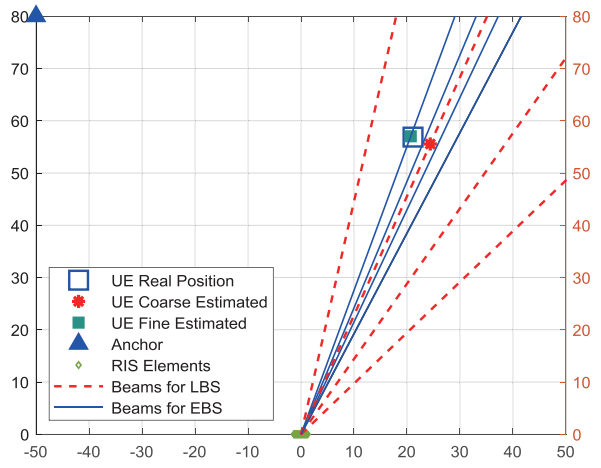

FIGURE 7. A snapshot of the proposed EBS model illustrates the refinement of the estimation.

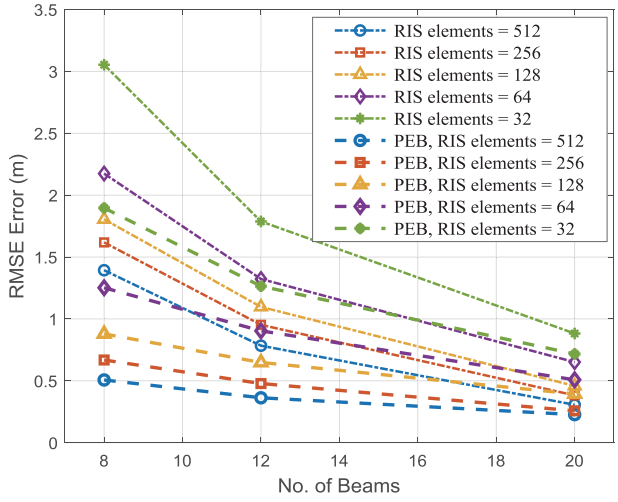

FIGURE 8. Localization error versus the number of beams for different number of RIS elements.

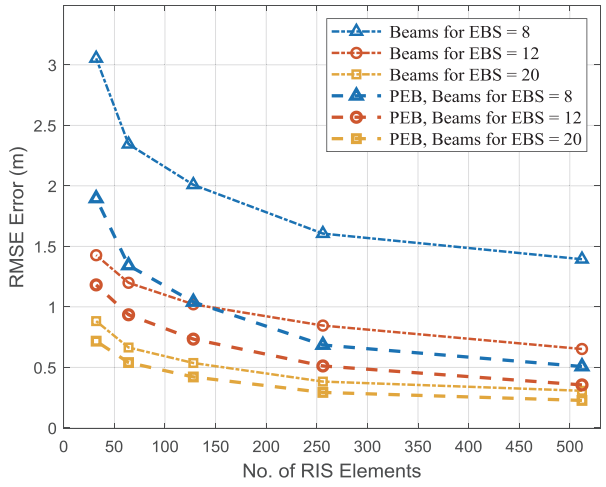

FIGURE 9. Localization error versus different number of RIS elements.

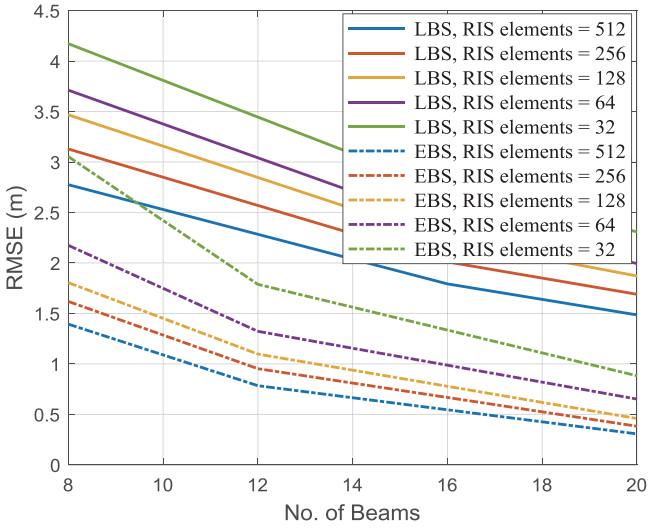

FIGURE 10. Localization error versus number of beams for LBS and the proposed EBS.

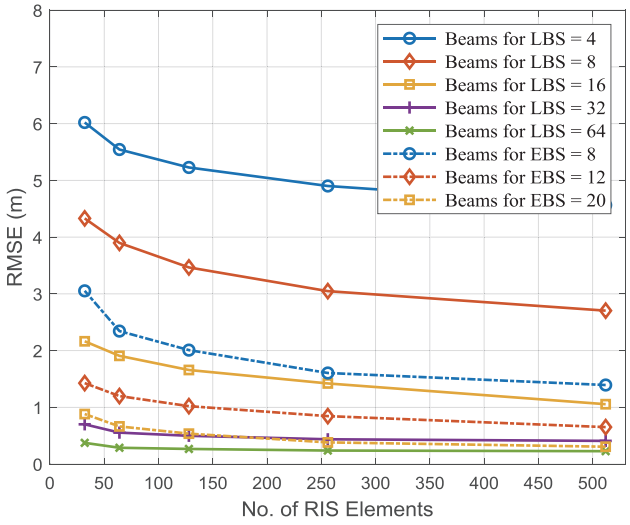

FIGURE 11. Comparation between RMSE of the proposed EBS with the LBS versus RIS elements.

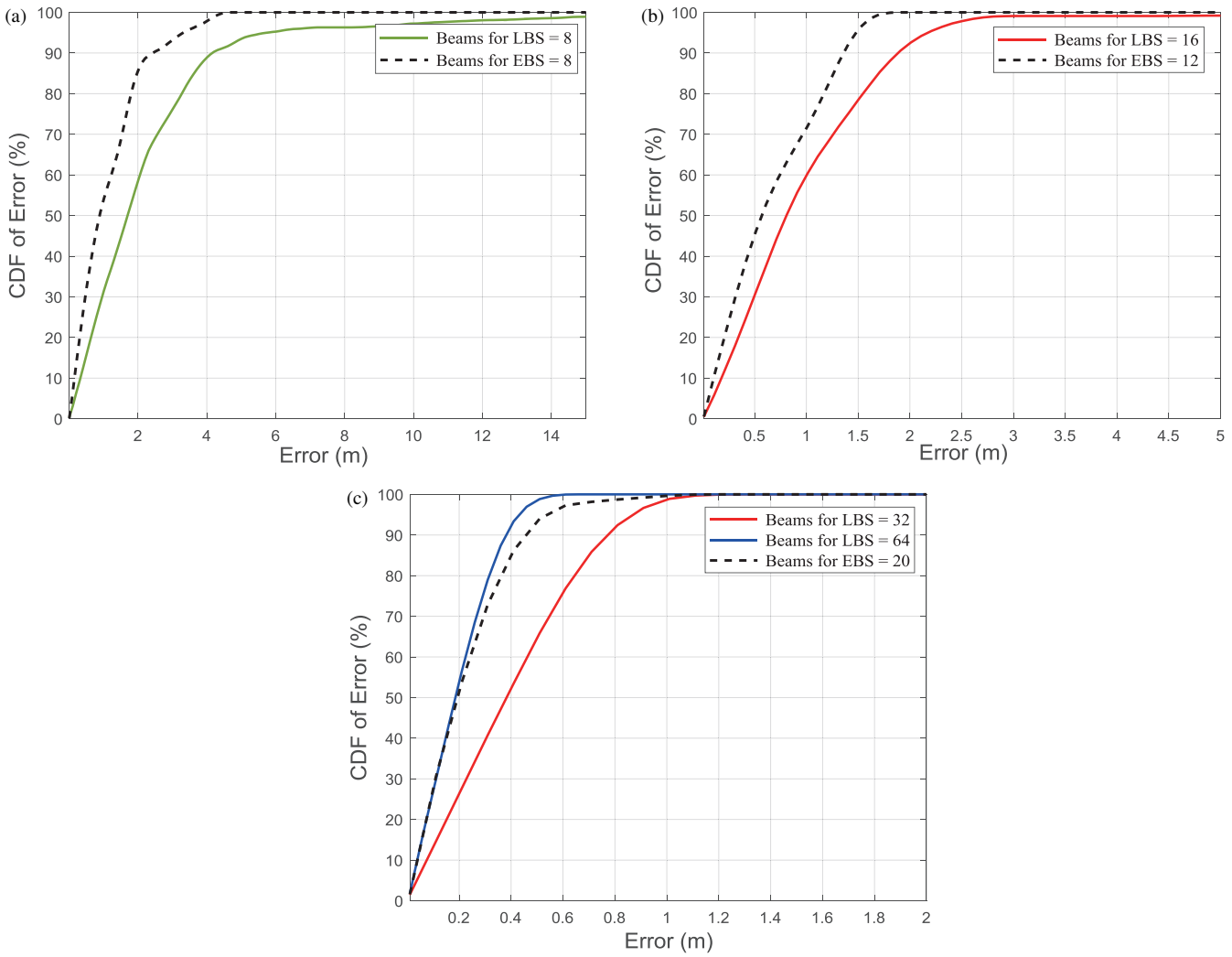

FIGURE 12. The CDFs of localization error using single-RIS of EBS compared with LBS for different numbers of beams.

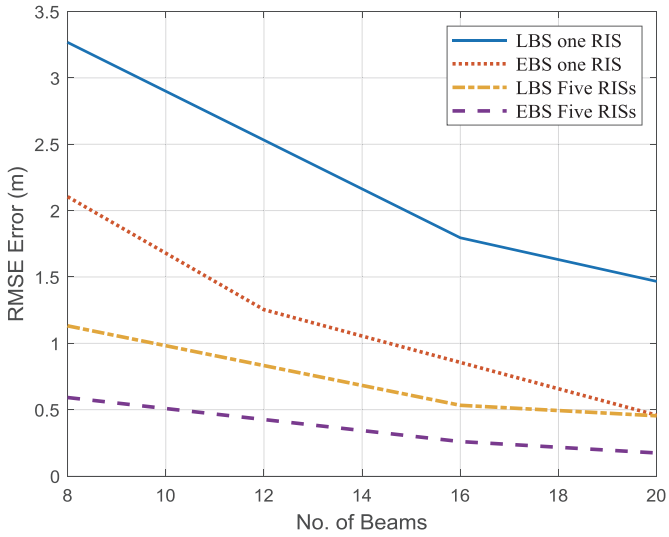

FIGURE 13. Comparation between single and multi RISs model using LBS and EBS.

tional LBS method. More specifically, when the same number of beams is used, for example 8 beams, in both LBS and EBS, the localization performance is enhanced by about 43%. While using 12 beams in EBS outperforms the performance of using 16 beams in LBS by about 40%, and also the localization error using 20 beams in EBS is almost identical to that of 32 beams in LBS. Interestingly in this case, the UE can be localized with an error lower than 35 cm when the number of RIS elements is 256 elements. The CDF of localization error in Figure 12(a) confirms the superiority of EBS method using 8 beams compared its corresponding beams in LBS. In Figure 12(b), the use of 12 beams in EBS outperforms the use of 16 in LBS. Finally in Figure 12(c), the use of 20 beams in EBS outperforms the use of 32 beams, and it is very close to the curve of 64 beams in LBS. The CDF curves indicate that 90% of estimation errors fall below 42 cm and 67% below 21 cm.

6.2.3. Performance of the Proposed EBS with Multi-RIS Model

Finally, based on Algorithm 2 in Subsection 3.3, the RMSE performance of the UE position estimation for multi-RIS modes using the proposed EBS method is depicted in Figure 13 and compared with other methods considered in this paper, from which we can note that the estimation error has been decreased interestingly to be about 55 cm using 8 beams and about 18 cm using only 20 beams in EBS method. It is worth mentioning that this figure was obtained using RISs, each with 128 elements.

7. CONCLUSION

A wireless localization system aided with multi-RIS is proposed in this paper leveraging ToA estimation and efficient beam sweeping scheme for the region of interest to estimate the AoDs for each RIS. The proposed EBS scheme for single and multi-RIS is compared with the conventional single RIS with LBS by evaluating the localization metric via numerical simulations and PEB benchmark. Simulation results demonstrate that the proposed EBS strategy enhances the positioning accuracy compared to LBS method using the same number of beams to scan the area of interest. Also, it is demonstrated that a sufficient number of beams is required to achieve precise localization accuracy while the number of RIS elements should be configured appropriately for fruitful scanning of the region of interest. Finally, the multi-RIS with EBS strategy has demonstrated superb localization accuracy compared with other schemes considered in this paper.

REFERENCES

[1] Zhao, S., Y. Liu, L. Wu, J. Rodriguez-Pifieiro, X. Yin, and J. Hong, "Recursive UE localization for a multi-RIS-assisted wireless system in an obstacle-dense environment," in *2023 17th European Conference on Antennas and Propagation, EuCAP*, Florence, Italy, Mar. 2023.

[2] Alhafid, A. K. and S. Younis, "Observed time difference of arrival based position estimation for LTE systems: Simulation framework and performance evaluation," *Eastern-European Journal of Enterprise Technologies*, Vol. 3, No. 9, 20–28, 2020.

[3] Zhang, H., N. Shlezinger, F. Guidi, D. Dardari, and Y. C. Eldar, "6G wireless communications: From far-field beam steering to near-field beam focusing," *IEEE Communications Magazine*, Vol. 61, No. 4, 72–77, 2023.

[4] Zhang, Z. and L. Dai, "Reconfigurable intelligent surfaces for 6G: Nine fundamental issues and one critical problem," *Tsinghua Science and Technology*, Vol. 28, No. 5, 929–939, 2023.

[5] Alhafid, A. K., S. Younis, and Y. E. M. Ali, "Efficient near-field localization aided with reconfigurable intelligent surface using geometric dilution of precision," *Journal of Information and Telecommunication*, 1–23, 2023.

[6] Wang, Z., Z. Liu, Y. Shen, A. Conti, and M. Z. Win, "Location awareness in beyond 5G networks via reconfigurable intelligent surfaces," *IEEE Journal on Selected Areas in Communications*, Vol. 40, No. 7, 2011–2025, 2022.

[7] Win, M. Z., Z. Wang, Z. Liu, Y. Shen, and A. Conti, "Location awareness via intelligent surfaces: A path toward holographic NLN," *IEEE Vehicular Technology Magazine*, Vol. 17, No. 2, 37–45, 2022.

[8] Dardari, D., N. Decarli, A. Guerra, and F. Guidi, "LOS/NLOS near-field localization with a large reconfigurable intelligent surface," *IEEE Transactions on Wireless Communications*, Vol. 21, No. 6, 4282–4294, 2022.

[9] Babu, B. A., P. R. Kalyan, V. V. Lakhmi, R. Reharika, and N. V. Raj, "An arduino-controlled reconfigurable intelligent surface with angular stability for 5G mmWave applications," *Progress In Electromagnetics Research Letters*, Vol. 114, 69–74, Nov. 2023.

[10] Zheng, B., C. You, W. Mei, and R. Zhang, "A survey on channel estimation and practical passive beamforming design for intelligent reflecting surface aided wireless communications," *IEEE Communications Surveys & Tutorials*, Vol. 24, No. 2, 1035–1071, 2022.

[11] Wu, Q. and R. Zhang, "Intelligent reflecting surface enhanced wireless network via joint active and passive beamforming," *IEEE Transactions on Wireless Communications*, Vol. 18, No. 11, 5394–5409, 2019.

[12] Liang, Y.-C., R. Long, Q. Zhang, J. Chen, H. V. Cheng, and H. Guo, "Large intelligent surface/antennas (LISA): Making reflective radios smart," *Journal of Communications and Information Networks*, Vol. 4, No. 2, 40–50, 2019.

[13] Dardari, D., N. Decarli, A. Guerra, and F. Guidi, "LOS/NLOS near-field localization with a large reconfigurable intelligent surface," *IEEE Transactions on Wireless Communications*, Vol. 21, No. 6, 4282–4294, 2022.

[14] Keykhosravi, K., M. F. Keskin, G. Seco-Granados, and H. Wymeersch, "SISO RIS-enabled joint 3D downlink localization and synchronization," in *ICC 2021 — IEEE International Conference on Communications*, 2021.

[15] Zhang, H., H. Zhang, B. Di, K. Bian, Z. Han, and L. Song, "Metalocalization: Reconfigurable intelligent surface aided multi-user wireless indoor localization," *IEEE Transactions on Wireless Communications*, Vol. 20, No. 12, 7743–7757, 2021.

[16] Ammous, M. and S. Valaee, "Cooperative positioning with the aid of reconfigurable intelligent surfaces and device-to-device communications in mmWave," in *2022 IEEE 33rd Annual International Symposium on Personal, Indoor and Mobile Radio Communications (PIMRC)*, 683–688, Kyoto, Japan, 2022.

[17] He, J., A. Fakhreddine, H. Wymeersch, and G. C. Alexandropoulos, "Compressed-sensing-based 3D localization with distributed passive reconfigurable intelligent surfaces," in *ICASSP 2023 - 2023 IEEE International Conference on Acoustics, Speech and Signal Processing (ICASSP)*, 1–5, 2023.

[18] Cheng, Q., L. Li, M.-M. Zhao, and M.-J. Zhao, "Cooperative localization for reconfigurable intelligent surface-aided mmWave systems," in *2022 IEEE Wireless Communications and Networking Conference (WCNC)*, 1051–1056, 2022.

[19] Wang, W. and W. Zhang, "Joint beam training and positioning for intelligent reflecting surfaces assisted millimeter wave communications," *IEEE Transactions on Wireless Communications*, Vol. 20, No. 10, 6282–6297, 2021.

[20] Li, K., M. El-Hajjar, and L.-L. Yang, "Reconfigurable intelligent surface aided position and orientation estimation based on joint beamforming with limited feedback," *IEEE Open Journal of the Communications Society*, Vol. 4, 748–767, 2023.

[21] Emenonye, D.-R., H. S. Dhillon, and R. M. Buehrer, "Fundamentals of RIS-aided localization in the far-field," *IEEE Transactions on Wireless Communications*, 2023.

[22] Keykhosravi, K., M. F. Keskin, S. Dwivedi, G. Seco-Granados, and H. Wymeersch, "Semi-passive 3D positioning of multiple RIS-enabled users," *IEEE Transactions on Vehicular Technology*, Vol. 70, No. 10, 11 073–11 077, 2021.

[23] He, J., H. Wymeersch, L. Kong, O. Silvén, and M. Juntti, "Large intelligent surface for positioning in millimeter wave MIMO systems]," in *2020 IEEE 91st Vehicular Technology Conference (VTC2020-Spring)*, 1–5, May 2020.

[24] He, J., H. Wymeersch, T. Sanguanpuak, O. Silvén, and M. Juntti, "Adaptive beamforming design for mmWave RIS-aided joint localization and communication," in *2020 IEEE Wireless Communications and Networking Conference Workshops (WCNCW)*, 1–6, 2020.

[25] De Lima, C., D. Belot, R. Berkvens, A. Bourdoux, D. Dardari, M. Guillaud, M. Isomursu, E.-S. Lohan, Y. Miao, A. N. Barreto, and e. al., "Convergent communication, sensing and localization in 6G systems: An overview of technologies, opportunities and challenges," *IEEE Access*, Vol. 9, 26 902–26 925, 2021.

[26] Elzanaty, A., A. Guerra, F. Guidi, and M.-S. Alouini, "Reconfigurable intelligent surfaces for localization: Position and orientation error bounds," *IEEE Transactions on Signal Processing*, Vol. 69, 5386–5402, 2021.

[27] Tran, L. C., A. T. Le, X. Huang, E. Dutkiewicz, D. Ngo, and A. Taparugssanagorn, "Complexity reduction for hybrid TOA/AOA localization in UAV-assisted WSNs," *IEEE Sensors Letters*, Vol. 7, No. 11, 2023.

[28] Ghazalian, R., H. Chen, G. C. Alexandropoulos, G. Seco-Granados, H. Wymeersch, and R. Jäntti, "Joint user localization and location calibration of a hybrid reconfigurable intelligent surface," *IEEE Transactions on Vehicular Technology*, 1–6, 2023.

[29] Wu, Q. and R. Zhang, "Beamforming optimization for wireless network aided by intelligent reflecting surface with discrete phase shifts," *IEEE Transactions on Communications*, Vol. 68, No. 3, 1838–1851, 2020.

[30] Al-Hourani, A., S. Chandrasekharan, and S. Kandeepan, "Path loss study for millimeter wave device-to-device communications in urban environment," in *2014 IEEE International Conference on Communications Workshops (ICC)*, 102–107, 2014.